THE JOURNAL OF PHYSICAL CHEMISTRY LETTERS
A JOURNAL OF THE AMERICAN CHEMICAL SOCIETY

pubs.acs.org/JPCL Letter

Predicting Mutation-Induced Changes in the Electronic Properties of Photosynthetic Proteins from First Principles: The Fenna–Matthews–Olson Complex Example

Yongbin Kim, Zach Mitchell, Jack Lawrence, Dmitry Morozov, Sergei Savikhin, and Lyudmila V. Slipchenko*

Cite This: J. Phys. Chem. Lett. 2023, 14, 7038–7044 Read Online

ACCESS | Metrics & More | Article Recommendations | Supporting Information

ABSTRACT: Multiscale molecular modeling is utilized to predict optical absorption and circular dichroism spectra of two single-point mutants of the Fenna–Matthews–Olson photosynthetic pigment–protein complex. The modeling approach combines classical molecular dynamics simulations with structural refinement of photosynthetic pigments and calculations of their excited states in a polarizable protein environment. The only experimental input to the modeling protocol is the X-ray structure of the wild-type protein. The first-principles modeling reproduces changes in the experimental optical spectra of the considered mutants, Y16F and Q198V. Interestingly, the Q198V mutation has a negligible effect on the electronic properties of the targeted bacteriochlorophyll *a* pigment. Instead, the electronic properties of several other pigments respond to this mutation. The molecular modeling demonstrates that a single-point mutation can induce long-range effects on the protein structure, while extensive structural changes near a pigment do not necessarily lead to significant changes in the electronic properties of that pigment.

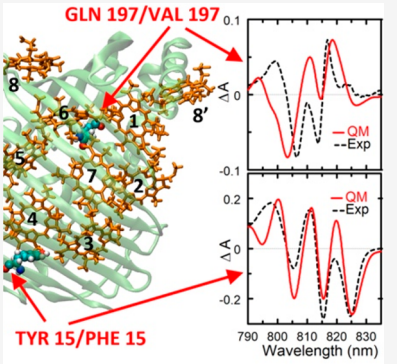

Nature perfected photosynthetic pigment–protein complexes over billions of years to achieve nearly 100% quantum efficiency in capturing sunlight. This incredible efficiency results from a precisely tuned interplay of positions, orientations, and electronic properties of light-absorbing molecules within a protein environment. While significant strides in understanding these complexes' energy transfer and conversion have been made through spectroscopic experimental data and X-ray structures, the detailed mechanistic picture of these processes often remains elusive. Many photosynthetic complexes contain tens or hundreds of pigments with overlapping electronic absorption, making it nearly impossible to resolve the properties of individual chromophores through optical experiments. To mitigate this complexity, point mutations of the protein sequence have been widely utilized as powerful tools for distinguishing the properties of individual pigments in a large photosynthetic complex. Changes in the optical spectra upon mutation are assumed to be dominated by the impact of the mutation site on the electronic properties of the closest pigment.[1] However, the assumption of a locality of the mutation-induced changes might not always be valid, introducing ambiguity into the interpretation of the optical experiments. In this paper, we investigate the impact of single-point mutations on the properties of individual pigments and optical spectra in the Fenna–Matthews–Olson (FMO) pigment–protein complex using multiscale molecular modeling.

A relatively simple structure coupled with complex excitonic interactions made the FMO complex a system of choice for developing new computational and spectroscopic techniques.[1−39] Found in green sulfur bacteria, it acts as an energy conduit between the chlorosomal antenna complex and the bacterial reaction center.[40,41] Each subunit of the homotrimeric FMO complex contains seven bacteriochlorophyll *a* (BChl *a*) pigments (Figure 1), with an eighth BChl *a* pigment bound between the subunits.[17] Close spacing of the pigments within each subunit leads to strong interpigment interactions and excitonic states delocalized across multiple pigments. Optical spectra and energy transfer dynamics in an excitonic system can be interpreted and modeled via an electronic Hamiltonian containing the information about the pigments' electronic excitation energies and couplings between the pigments. Over the years, several empirical Hamiltonians of the FMO complex have been developed via a combination of structural information and fitting to spectroscopic data.[12,14,16,18,20,24,25,29,31]

Received: May 27, 2023
Accepted: July 26, 2023

https://doi.org/10.1021/acs.jpclett.3c01461
J. Phys. Chem. Lett. 2023, 14, 7038–7044

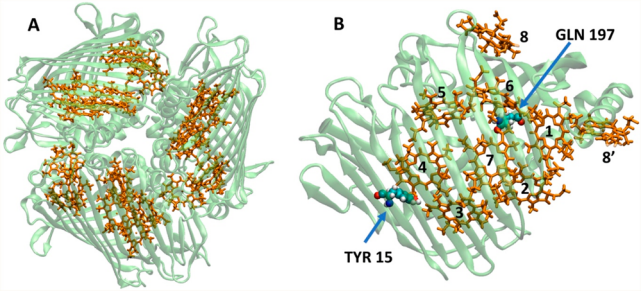

Figure 1. (A) Fenna−Matthews−Olson (FMO) pigment−protein complex. (B) Monomer subunit of FMO with the sites of single-point mutations considered in this work.

A number of single-point and double FMO mutants targeting the electronic properties of individual pigments and the structural integrity of the complex have been synthesized.[1,42−48] For example, Saer et al. engineered and characterized eight site-directed mutants in which changes were introduced into protein pockets housing each FMO pigment.[1] It was shown that in all but one mutant the associated changes in absorption and circular dichroism (CD) spectra could be modeled by a spectral shift of the excitation energy of the specific pigment targeted by a mutation. For the mutation near pigment 7 (Q198V), however, such a simple model could not account for the spectral changes. It was suggested, therefore, that either the proposed earlier Hamiltonians improperly assign the spectral position of the respective pigment or the particular mutation near pigment 7 affects the electronic properties of other pigments via long-distance structural changes.[1] This work sheds light on this puzzle using first-principles-based molecular modeling.

In our recent work, we have developed a multiscale computational workflow that provided an excellent agreement between modeled and experimental absorption and CD spectra of the wild-type FMO complex.[4] This computational approach combines classical molecular dynamics simulations of the whole complex with a series of quantum mechanics/molecular mechanics (QM/MM) optimizations of pigment structures and polarizable QM/MM calculations of pigment excitation energies and transition charges. Notably, the only experimental input to the computational workflow is the initial X-ray structure of the protein. The average electronic Hamiltonian produced by this modeling is in qualitative agreement with the commonly accepted empirical Hamiltonians.[4] In this Letter, we extend this methodology to modeling optical properties of the FMO complexes with point mutations introduced near BChl *a* pigment 3 (Y16F) and near pigment 7 (Q198V), later termed "mutant 3" and "mutant 7", respectively.

The initial structures of the mutated FMO complexes were created from the wild-type FMO structure [Protein Data Bank (PDB) entry 3ENI[17]] by substituting respective amino acids. Note that this paper follows the protein numbering scheme provided in PDB entry 3ENI, while the mutant numbering used in ref 1 is shifted from the PDB scheme by +1; i.e., mutants denoted as Y16F and Q198V in ref 1 correspond to Tyr 15/Phe 15 and Gln 197/Val 197 substitutions in the PDB structure, respectively. The rest of the computational methodology closely follows the methodology developed and described in ref 4, the only difference being that the quantum mechanical (QM) regions in the QM/MM geometry optimization step include full BChl *a* molecules in this work, while the phytol tails were truncated between C3 and C5 in ref 4. Briefly, the computational methodology includes the following steps: equilibration of the solvated protein structures using classical molecular dynamics (MD), selection of 100 random structures from the MD trajectory, correction of the pigment geometries with constrained QM/MM geometry optimizations at the PBE0/6-31G* level of theory, and calculations of the electronic transition energies and transition charges for each of the eight pigments with the polarizable QM/EFP (effective fragment potential) method[49−56] at the TDDFT PBE0/6-31G* level of theory at each of the selected structures. We note that TDDFT PBE0 has been shown to accurately describe the Q_y excited states of BChl *a* pigments.[26,57] Pigments' electronic transition energies and transition charges for each structure are combined to build individual electronic Hamiltonians, whose eigenvalues and eigenvectors provide positions and intensities for the peaks in the absorption and CD spectra. Averaging the individual snapshot spectra results in the total absorption and CD spectra of the mutated complexes. Further details of the computational procedure can be found in the Supporting Information and in ref 4.

We note that all steps of the computational procedure listed above are essential for the accurate modeling of the optical properties of the FMO complex. Specifically, in ref 4, we demonstrated that it is possible to obtain meaningful optical spectra of FMO only by accounting for thermal fluctuations of the protein and proper statistical averaging, as the spectra computed for the individual structural snapshots are dramatically different from each other and the experimental spectra. Constrained QM/MM geometry optimizations are necessary for correcting inaccuracies of the force field in predicting internal structures and strong H-bonds of BChl pigments with neighboring amino acids. Finally, a polarizable description of the protein with the EFP force field that accounts for the secondary electric field mutually induced by charged or polar moieties on BChl *a* pigments and vice versa proved to be a critical element for achieving quantitative accuracy in predicting relative site energies of different pigments.

Table 1 shows the average Hamiltonian computed from 100 structural snapshots of the wild-type FMO complex. Diagonal elements H_{ii} represent electronic transition energies of pigments *i*, while off-diagonal elements H_{ij} represent excitonic couplings between pigments *i* and *j* computed using TrEsp

Table 1. Average Electronic Hamiltonian of the Wild-Type FMO Complex[a]

BChl 1	BChl 2	BChl 3	BChl 4	BChl 5	BChl 6	BChl 7	BChl 8′
12373 (69)	-109 (6.7)	5.2 (0.5)	-6.4 (0.5)	6.5 (0.7)	-9.2 (3.6)	-2.6 (1.4)	23 (4.3)
-109 (6.7)	**12544**(112)	37 (1. 9)	9.4 (0.8)	1.6 (0.8)	12 (1.4)	6.7 (2.1)	5.7 (1.5)
5.2 (0.5)	37 (1.9)	**12166** (86)	-50 (7.4)	-1.8 (1.1)	-10 0.5)	6.7 4.3)	1.4 (0.3)
-6.4 (0.5)	9.4 (0.8)	-50 (7.4)	**12326** (81)	-83 (6.5)	-19 (1.3)	-54 6.3)	-2.0 (0.2)
6.5 (0.7)	1.6 (0.8)	-1.8 (1.1)	-83 (6.5)	**12463** (90)	54 (7.1)	4.2 (2.6)	4.4 (0.3)
-9.2 (3.6)	12 (1.4)	-10 (0.5)	-19 (1.3)	54 (7.1)	**12450** (74)	29 (4.0)	-12 (1.2)
-2.6 (1.4)	6.7 (2.1)	6.7 (4.3)	-54 (6.3)	4.2 (2.6)	29 (4.0)	**12354** (57)	-14 (0.8)
23 (4.3)	5.7 (1.5)	1.4 (0.3)	-2.0 (0.2)	4.4 (0.3)	-12 (1.2)	-14 (0.8)	**12412** (142)

[a]The values in parentheses represent RMSDs for each value computed over 100 structural snapshots of the MD trajectory. Diagonal energies are shifted by −2420 cm^{-1} to match the experimental absorption spectrum. All values are in inverse centimeters.

https://doi.org/10.1021/acs.jpclett.3c01461
J. Phys. Chem. Lett. 2023, 14, 7038−7044

transition charges on pigment atoms (see the details of computing electronic couplings in the Supporting Information). The root-mean-square deviations (RMSDs) of the excitation energies and couplings (shown in parentheses in Table 1) reflect the effect of thermal fluctuation of the protein. Table 2 shows deviations between the wild-type average

Table 2. Deviations in the Average Values of the Hamiltonians of Mutants 3 and 7 with Respect to the Average Values of the Wild-Type Hamiltonian[a]

Mutant 3							
BChl 1	BChl 2	BChl 3	BChl 4	BChl 5	BChl 6	BChl 7	BChl 8
-2.3±9.4	-7.7±1.2	1.1±0.1	-1.3±0.1	1.9±0.1	-4.9±0.5	-4.1±.5	13±.6
	22±17	-0.1±0.3	-0.6±0.1	-0.4±0.1	0.9±0.2	2.3±0.3	3.6±0.2
		273±12	5.4±0.1	0.7±0.1	-0.6±0.1	9.8±0.8	0.7±0.1
49.4±8.5			-34±12	-5.9±0.8	-0.6±0.2	8.6±0.9	0.2±0.1
-22±1.1	37.3±15			2.7±14	11±1.1	-1.4±0.3	0.1±0.1
1.3±0.1	1±0.3	38.2±13			-74±11	2.4±0.6	2.6±0.2
-0.8±0.1	-1.7±0.1	-8.2±1	-46.2±10			20±10	1.2±0.1
1±0.1	0.5±0.1	0.9±0.1	-5.4±0.6	66±11			42±20
-1.2±0.5	0.7±0.2	-0.5±0.1	-1.3±0.2	11±1	-78±12		
-1.1±0.2	3.3±0.3	4.5±0.8	7.9±0.9	-0.7±0.4	8.1±0.6	-9.4±11	
4.6±0.6	3.2±0.2	0.7±0.1	-0.3±0.1	0.4±0.1	-0.3±0.2	-0.8±0.1	29±21
BChl 1	BChl 2	BChl 3	BChl 4	BChl 5	BChl 6	BChl 7	BChl 8
Mutant 7							

[a]Uncertainties of each value are denoted with ±. All values are in inverse centimeters.

Hamiltonian and the Hamiltonians of mutants 3 and 7. The uncertainties of each value are also provided. Distributions of pigment excitation energies in the Y16F and Q198V mutants are also shown in Figures S3 and S4.

Panels A and B of Figure 2 compare computed and experimental absorption and CD spectra of the wild-type FMO complex. As in our previous work,[4] the computational model captures all major features of the experimental absorption and CD spectra of the wild-type FMO complex. Panels C−F of Figure 2 depict spectral changes predicted for both mutants and experimentally measured data published previously.[1] Absorption and CD spectra of mutants are shown in Figures S5 and S6. The agreement between first-principles modeling and experiment is quite good, with all significant measured features present. It is noteworthy that in the case of mutant 7, a simplistic empirical approach used in ref 1 in which the mutation induces an electrochromic shift only to the nearby pigment (i.e., a "local model") fails to reproduce measured spectral differences. In contrast, the first-principles modeling reproduces both absorption and CD changes remarkably well. The underlying reason for the failure of the local model becomes evident upon inspection of the effect of this mutation on the system Hamiltonian (Table 2). Indeed, explicit electronic structural modeling predicts that the Q198V mutation near BChl 7 causes a negligible excitation energy shift in this pigment ($\Delta H_{77} = -9 \pm 11$ cm^{-1}); i.e., the targeted site is barely affected by the mutation. It is surprising, however, that all other pigments are affected by this mutation to a more significant extent, with the largest shifts predicted for pigments 6, 5, and 1 ($\Delta H_{66} = 76 \pm 12$ cm^{-1}, $\Delta H_{55} = 66 \pm 11$ cm^{-1}, and $\Delta H_{11} = 49 \pm 8$ cm^{-1}). On the contrary, electronic structure modeling of mutant 3 predicts a major spectral shift of targeted pigment 3 ($\Delta H_{33} = 273 \pm 12$ cm^{-1}), with shifts of other pigments being at least 4 times smaller (Table 2). Consistent with this analysis, the local model, in which only the nearest pigment 3 is assumed to be affected by the Y16F mutation, reproduces experimental data reasonably well.[1]

The observed nonlocality of energetic shifts in mutant 7 suggests that the single-point Q198V mutation induces long-

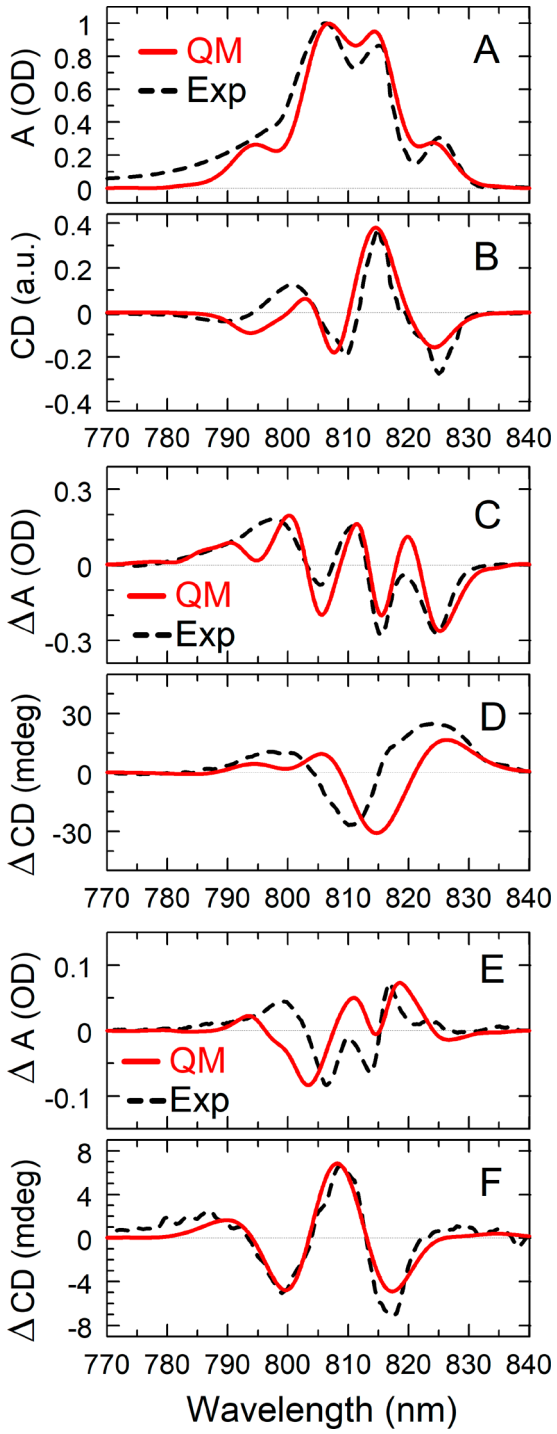

Figure 2. (A) Absorption and (B) CD spectra of the wild-type FMO complex. (C−F) Absorption and CD differences for the Y16F and Q198V mutants from the wild-type spectra. Black dashed lines represent spectra measured experimentally in ref 1, and red lines are spectra calculated from the QM modeling as described in the text.

range structural rearrangements of the protein scaffold. For example, pigments 1 and 5, whose site energies are significantly affected by the mutation, are located ∼20 and ∼12 Å, respectively, from the mutation site (as measured between the closest non-hydrogen atoms of the mutated amino acid and BChl *a* head), beyond the direct reach of a possible electrochromic effect due to a substitution of polar glutamine with nonpolar valine. It should be noted, however, that both

https://doi.org/10.1021/acs.jpclett.3c01461
J. Phys. Chem. Lett. 2023, 14, 7038−7044

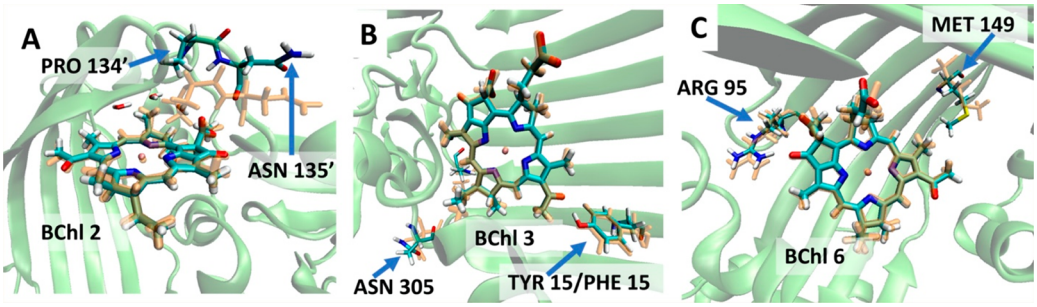

Figure 3. Structural changes in the Y16F (Tyr 15/Phe 15) mutant. (A) Significant structural changes near pigment 2. Minor structural changes near (B) mutated site 3 and (C) site 6. Primed numbers (Pro 134′ and Asn 135′) label amino acids belonging to the neighboring protein subunit. The wild-type protein is shown as a light-green ribbon. Wild-type amino acids and BChl *a* heads are shown in color. The corresponding amino acids in the Y16F mutant are in light orange.

optical measurements and molecular modeling suggest that the overall secondary protein structure in mutants is well preserved. For example, changes in electronic interpigment couplings ($H_{i\neq j}$) that reflect the relative position and orientation of the pigments are small and have negligible effects on the spectral changes observed in both mutants.

A summary of energetic changes due to mutations (Table 2) suggests that a single-point mutation might produce both local and long-range effects, the former arising due to the electrochromic effect of a substituted amino acid and the latter arising from structural distortions in the protein scaffold. A similar conclusion was also derived from the analysis of hole-burning spectra of FMO mutants.[43,44] However, molecular modeling provides a unique means for the analysis of how the mutation-induced changes in the protein structure are translated into the spectral properties of the mutants. To support this discussion, the most significant structural rearrangements in mutants are shown in Figures 3 and 4.

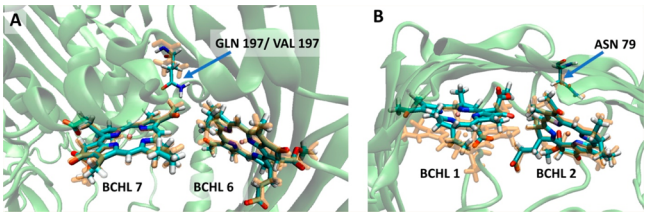

Figure 4. Structural changes caused by the Q198V (Gln 197/Val 197) mutation near (A) mutated site 7 and (B) sites 1 and 2. See the legend of Figure 3 for the color-coding scheme.

By far, the most noticeable effect of the Y16F mutation is on the properties of pigment 3, whose transition energy shifts by ΔH_{33} = +273 cm^{-1}. This dramatic spectral shift can be attributed to breaking the H-bond to the pigment's C3 acetyl group upon substituting tyrosine with phenylalanine. The oxygen atom of the C3 acetyl accumulates an excess electron density in the Q_y excited state of BChl *a* (see detachment and attachment electron density plots in Figure S7). When the acetyl oxygen is H-bonded to tyrosine, some of this excess electron density in the excited state is donated to the H-bond, leading to stabilization (red-shift) of the excited state. In the absence of the H-bond (as in the case of the Y16F mutant), the excited state on pigment 3 becomes effectively blue-shifted, with respect to the wild type.

Quite surprisingly, single-point mutation Y16F led to a sizable energetic shift of −70 cm^{-1} in pigment 6 (Figure 3C). As the closest-atom separation between pigment 6 and the mutation site exceeds 25 Å, this spectral shift cannot be explained by the electrochromic effect, which decays as approximately R^3 with distance. Our analysis suggests that the observed spectral shift is driven by slight structural distortions in a cluster of several closely lying polar amino acids (Met 149, Gln 197, and Asp 146) and the charged Arg 95 that forms an H-bond with the keto group of pigment 6. Even minor distortions or displacements of these amino acids might result in non-negligible changes in the electric field at pigment 6 and thus cause the observed shift in its transition energy.

One of the most remarkable findings of this study is that in both mutants we have observed noticeable structural changes near all pigments (as measured, for example, by changes in the average closest separations between particular residues and BChl *a* pigments or as the RMSD in the internal structures of residues). However, only some structural changes lead to distinguishable energetic and spectral shifts. Indeed, most structural changes in mutants occur in more flexible protein regions. In contrast, the parts of the protein with well-defined secondary structures (β-sheets and α-helices) are less affected by single-point mutations. As one example of this observation, some of the most extensive structural distortions in the Y16F mutant are observed in a nonstructured protein region near pigment 2, with the neighboring subunit's amino acids Pro 134′ and Asn 135′ shifted by ∼2 Å with respect to pigment 2 (Figure 3A). Notably, this structural shuffle in the Y16F mutant is responsible for closing a water channel that in the wild type connects the water molecule coordinating Mg of pigment 2 with the external water solvent. As shown in Figure 3A, all water is expelled from a pigment 2 pocket in the Y16F mutant. However, these seemingly drastic structural rearrangements near pigment 2 result in a negligible energetic shift (ΔH_{22} = 20 ± 10 cm^{-1}). Similarly, pigment 5 is located near a non-ordered protein chain, where several amino acids in the Y16F mutant undergo substantial changes in their average orientations or separation from the pigment [Ser 244, Lys 246, and Pro 250 (see Figure S8)]. Nevertheless, similar to the case of pigment 2, these fluctuations do not result in a significant energetic shift of pigment 5.

In general, it is expected that substantial fluctuations in the positions of charged and polar amino acids should result in a notable change in the electric field at the location of a chromophore and lead to the electro- or solvatochromic shift of its transition energy. On the contrary, striking changes in the average positions of multiple charged/polar amino acids have negligible effects on the spectral properties of pigments 2 and

https://doi.org/10.1021/acs.jpclett.3c01461
J. Phys. Chem. Lett. 2023, 14, 7038−7044

5. We suggest that the observed muted effect of unstructured regions of the protein on the spectral properties of nearby chromophores is a beneficial evolutionary trait that prevents the excessive modulation of pigment transition energies by the thermal motion of the protein that could otherwise affect the efficiency of energy transfer. The electric field of the peripheral residues in unstructured stretches of the protein could be effectively screened by nearby water molecules or canceled out by a concerted motion of nearby oppositely charged residues.

Substitution of glutamine with valine in the Q198V mutant (see Figure 4A) does not significantly affect the transition properties of the neighboring pigment 7 as neither of the amino acids participates in H-bonding or induces a sufficiently different electric field at this pigment. However, this single-point mutation in the middle of the protein scaffold produces subtle structural distortions to the whole protein, which collectively shift the site energies of all of the other pigments. As a result, the effect of this mutation on the optical and energetic properties of the protein cannot be predicted by a local empirical model (there is no single dominating effect but rather a combination of minor effects that might cancel each other). Despite this challenge, computational modeling based on structures extracted from classical MD trajectories reproduces the main features of the experimental absorption and CD spectra quite well. Figure 4 shows some of the observed structural distortions in Q198V.

Like in the Y16F mutant, the protein region near pigment 2 appears to be strongly affected by the Q198V mutation. However, in the Q198V mutant, despite many observed structural deformations (see an example of shifted Asn 79 in Figure 4B), the water channel near pigment 2 remains active. On the contrary, a relative orientation of pigments 1 and 2 in the Q198V mutant is noticeably distorted; e.g., the average distance between Mg atoms of pigments 1 and 2 decreases by ∼0.4 Å in Q198V with respect to that in the wild type (see Figure 4B), changing the electronic coupling between these pigments by −22 cm^{-1}. Also, similar to the Y16F mutant, the transition energy of pigment 6 in Q198V is strongly influenced by fluctuations of nearby Arg 95 and by the electrochromic effect of the mutated site (Figure 4A), with the total electrochromic shift of −77 cm^{-1}.

Using the example of the FMO pigment−protein complex, we demonstrate that the developed first-principles-based modeling protocol is a powerful tool enabling quantitative prediction and mechanistic analysis of changes in the electronic and optical properties of photosynthetic chromophores caused by point mutations. The mutation engineered to target properties of a particular pigment might nevertheless have a minimal effect on that pigment and, instead, affect the electronic properties of distant chromophores. Our analysis also suggests that extensive mutation-induced structural changes near a pigment do not necessarily cause significant changes in the spectral properties of that pigment; i.e., a purely structural analysis of the mutation is not sufficient for understanding the changes occurring in optical spectra. The multiscale molecular modeling protocol reported here could serve as a basis for the intelligent design of mutations with a desired targeted effect on specific components of a pigment−protein complex.

■ ASSOCIATED CONTENT

Supporting Information

The Supporting Information is available free of charge at https://pubs.acs.org/doi/10.1021/acs.jpclett.3c01461.

Description of the computational methodology, including schemes for separating the system into QM and MM regions, figures showing the distribution of excitation energies, absorption and CD spectra of FMO mutants, detachment−attachment electron density plot of BChl *a*, and a figure demonstrating structural rearrangements near BChl *a* 5 in the Y16F mutant (PDF)

■ AUTHOR INFORMATION

Corresponding Author

Lyudmila V. Slipchenko − *Department of Chemistry, Purdue University, West Lafayette, Indiana 47907, United States;* orcid.org/0000-0002-0445-2990; Email: lslipchenko@purdue.edu

Authors

Yongbin Kim − *Department of Chemistry, Purdue University, West Lafayette, Indiana 47907, United States*

Zach Mitchell − *Department of Physics and Astronomy, Purdue University, West Lafayette, Indiana 47907, United States*

Jack Lawrence − *Department of Chemistry, Purdue University, West Lafayette, Indiana 47907, United States*

Dmitry Morozov − *Nanoscience Center and Department of Chemistry, University of Jyväskylä, 40014 Jyväskylä, Finland;* orcid.org/0000-0001-9524-948X

Sergei Savikhin − *Department of Physics and Astronomy, Purdue University, West Lafayette, Indiana 47907, United States*

Complete contact information is available at: https://pubs.acs.org/10.1021/acs.jpclett.3c01461

Notes

The authors declare no competing financial interest.

■ ACKNOWLEDGMENTS

J.L. and L.V.S. gratefully acknowledge support from the National Science Foundation (Grant CHE-2102639). Y.K., J.L., Z.M., S.S., and L.V.S. acknowledge support from the Department of Energy, Office of Basic Energy Sciences (Grant DE-SC0018239). D.M. acknowledges funding from the Academy of Finland (Grant 332743). This research was partly supported through computational resources provided by Information Technology at Purdue University.

■ REFERENCES

(1) Saer, R. G.; Stadnytskyi, V.; Magdaong, N. C.; Goodson, C.; Savikhin, S.; Blankenship, R. E. Probing the Excitonic Landscape of the Chlorobaculum Tepidum Fenna-Matthews-Olson (FMO) Complex: A Mutagenesis Approach. *Biochim. Biophys. Acta - Bioenerg.* **2017**, *1858*, 288−296.

(2) Buck, D. R.; Savikhin, S.; Struve, W. S. Effect of Diogonal Energy Disorder on Circular Dichroism Spectra of Fenna-Matthews-Olson Trimers. *J. Phys. Chem. B* **1997**, *101*, 8395−8397.

(3) Buck, D. R.; Savikhin, S.; Struve, W. S. Ultrafast Absorption Difference Spectra of the FMO Protein at 19 K: Experiment and Simulations. *Biophys. J.* **1997**, *72*, 24−36.

(4) Kim, Y.; Morozov, D.; Stadnytskyi, V.; Savikhin, S.; Slipchenko, L. V. Predictive First-Principles Modeling of a Photosynthetic

Antenna Protein: The Fenna−Matthews−Olson Complex. *J. Phys. Chem. Lett.* **2020**, *11*, 1636−1643.
(5) Savikhin, S.; Buck, D. R.; Struve, W. S. Oscillating Anisotropies in a Bacteriochlorophyll Protein: Evidence for Quantum Beating between Exciton Levels. *Chem. Phys.* **1997**, *223*, 303−312.
(6) Savikhin, S.; Buck, D. R.; Struve, W. S. Pump-Probe Anisotropies of Fenna-Matthews-Olson Protein Trimers from *Chlorobium Tepidum*: A Diagnostic for Exciton Localization? *Biophys. J.* **1997**, *73*, 2090−2096.
(7) Savikhin, S.; Buck, D. R.; Struve, W. S. Toward Level-to-Level Energy Transfers in Photosynthesis: The Fenna-Matthews-Olson Protein. *J. Phys. Chem. B* **1998**, *102*, 5556−5565.
(8) Savikhin, S.; Buck, D. R.; Struve, W. S. The Fenna-Matthews-Olson Protein: A Strongly Coupled Photosynthetic Antenna. In *Resonance Energy Transfer*; Andrews, D. L., Demidov, A. A., Eds.; John Wiley & Sons: New York, 1999; pp 399−434.
(9) Savikhin, S.; Struve, W. S. Ultrafast Energy Transfer in Fmo Trimers from the Green Bacterium Chlorobium Tepidum. *Biochem* **1994**, *33*, 11200−11208.
(10) Savikhin, S.; Struve, W. S. Low-Temperature Energy Transfer in Fmo Trimers from the Green Photosynthetic Bacterium Chlorobium Tepidum. *Photosynth. Res.* **1996**, *48*, 271−276.
(11) Louwe, R. J. W.; Vrieze, J.; Hoff, A. J.; Aartsma, T. J. Toward an Integral Interpretation of the Optical Steady-State Spectra of the Fmo-Complex of Prosthecochloris Aestuarii. 2. Exciton Simulations. *J. Phys. Chem. B* **1997**, *101*, 11280−11287.
(12) Vulto, S. I. E.; de Baat, M. A.; Louwe, R. J. W.; Permentier, H. P.; Neef, T.; Miller, M.; van Amerongen, H.; Aartsma, T. J. Exciton Simulations of Optical Spectra of the Fmo Complex from the Green Sulfur Bacterium Chlorobium Tepidum at 6 K. *J. Phys. Chem. B* **1998**, *102*, 9577−9582.
(13) Vulto, S. I. E.; de Baat, M. A.; Neerken, S.; Nowak, F. R.; van Amerongen, H.; Amesz, J.; Aartsma, T. J. Excited State Dynamics in Fmo Antenna Complexes from Photosynthetic Green Sulfur Bacteria: A Kinetic Model. *J. Phys. Chem. B* **1999**, *103*, 8153−8161.
(14) Brixner, T.; Stenger, J.; Vaswani, H. M.; Cho, M.; Blankenship, R. E.; Fleming, G. R. Two-Dimensional Spectroscopy of Electronic Couplings in Photosynthesis. *Nature* **2005**, *434*, 625−628.
(15) Olson, J. The FMO Protein. In *Discoveries in Photosynthesis*; Govindjee, Beatty, J. T., Gest, H., Allen, J., Eds.; Springer Netherlands: Dordrecht, The Netherlands, 2005; Vol. *20*, pp 421−427.
(16) Adolphs, J.; Muh, F.; Madjet, M. E. A.; Renger, T. Calculation of Pigment Transition Energies in the Fmo Protein. *Photosynth. Res.* **2008**, *95*, 197−209.
(17) Tronrud, D. E.; Wen, J. Z.; Gay, L.; Blankenship, R. E. The Structural Basis for the Difference in Absorbance Spectra for the Fmo Antenna Protein from Various Green Sulfur Bacteria. *Photosynth. Res.* **2009**, *100*, 79−87.
(18) Milder, M. T. W.; Bruggemann, B.; van Grondelle, R.; Herek, J. L. Revisiting the Optical Properties of the Fmo Protein. *Photosynth. Res.* **2010**, *104*, 257−274.
(19) Moix, J.; Wu, J.; Huo, P.; Coker, D.; Cao, J. Efficient Energy Transfer in Light-Harvesting Systems, III: The Influence of the Eighth Bacteriochlorophyll on the Dynamics and Efficiency in Fmo. *J. Phys. Chem. Lett.* **2011**, *2*, 3045−3052.
(20) Olbrich, C.; Jansen, T. L. C.; Liebers, J.; Aghtar, M.; Strumpfer, J.; Schulten, K.; Knoester, J.; Kleinekathofer, U. From Atomistic Modeling to Excitation Transfer and Two-Dimensional Spectra of the Fmo Light-Harvesting Complex. *J. Phys. Chem. B* **2011**, *115*, 8609−8621.
(21) Olbrich, C.; Strumpfer, J.; Schulten, K.; Kleinekathofer, U. Quest for Spatially Correlated Fluctuations in the Fmo Light-Harvesting Complex. *J. Phys. Chem. B* **2011**, *115*, 758−764.
(22) Schmidt am Busch, M.; Müh, F.; El-Amine Madjet, M.; Renger, T. The Eighth Bacteriochlorophyll Completes the Excitation Energy Funnel in the Fmo Protein. *J. Phys. Chem. Lett.* **2011**, *2*, 93−98.
(23) Wen, J.; Zhang, H.; Gross, M. L.; Blankenship, R. E. Native Electrospray Mass Spectrometry Reveals the Nature and Stoichiometry of Pigments in the Fmo Photosynthetic Antenna Protein. *Biochem* **2011**, *50*, 3502−3511.
(24) Fidler, A. F.; Caram, J. R.; Hayes, D.; Engel, G. S. Towards a Coherent Picture of Excitonic Coherence in the Fenna-Matthews-Olson Complex. *J. Phys. B: At., Mol. Opt. Phys.* **2012**, *45*, 154013.
(25) Gao, J. K.; Shi, W. J.; Ye, J.; Wang, X. Q.; Hirao, H.; Zhao, Y. QM/MM Modeling of Environmental Effects on Electronic Transitions of the Fmo Complex. *J. Phys. Chem. B* **2013**, *117*, 3488−3495.
(26) List, N. H.; Curutchet, C.; Knecht, S.; Mennucci, B.; Kongsted, J. Toward Reliable Prediction of the Energy Ladder in Multi-chromophoric Systems: A Benchmark Study on the Fmo Light-Harvesting Complex. *J. Chem. Theory Comput.* **2013**, *9*, 4928−4938.
(27) Jurinovich, S.; Curutchet, C.; Mennucci, B. The Fenna-Matthews-Olson Protein Revisited: A Fully Polarizable (TD)DFT/MM Description. *ChemPhysChem* **2014**, *15*, 3194−3204.
(28) Chandrasekaran, S.; Aghtar, M.; Valleau, S.; Aspuru-Guzik, A.; Kleinekathöfer, U. Influence of Force Fields and Quantum Chemistry Approach on Spectral Densities of BChl *a* in Solution and in Fmo Proteins. *J. Phys. Chem. B* **2015**, *119*, 9995−10004.
(29) Jia, X. Y.; Mei, Y.; Zhang, J. Z. H.; Mo, Y. Hybrid QM/MM Study of Fmo Complex with Polarized Protein-Specific Charge. *Sci. Rep.* **2015**, *5*, 17096.
(30) Higashi, M.; Saito, S. Quantitative Evaluation of Site Energies and Their Fluctuations of Pigments in the Fenna-Matthews-Olson Complex with an Efficient Method for Generating a Potential Energy Surface. *J. Chem. Theory Comput.* **2016**, *12*, 4128−4137.
(31) Kell, A.; Blankenship, R. E.; Jankowiak, R. Effect of Spectral Density Shapes on the Excitonic Structure and Dynamics of the Fenna-Matthews-Olson Trimer from Chlorobaculum Tepidum. *J. Phys. Chem. A* **2016**, *120*, 6146−6154.
(32) Schulze, J.; Shibl, M. F.; Al-Marri, M. J.; Kühn, O. Multi-Layer Multi-Configuration Time-Dependent Hartree (ML-MCTDH) Approach to the Correlated Exciton-Vibrational Dynamics in the Fmo Complex. *J. Chem. Phys.* **2016**, *144*, 185101.
(33) Padula, D.; Lee, M. H.; Claridge, K.; Troisi, A. Chromophore-Dependent Intramolecular Exciton−Vibrational Coupling in the Fmo Complex: Quantification and Importance for Exciton Dynamics. *J. Phys. Chem. B* **2017**, *121*, 10026−10035.
(34) Kim, C. W.; Choi, B.; Rhee, Y. M. Excited State Energy Fluctuations in the Fenna-Matthews-Olson Complex from Molecular Dynamics Simulations with Interpolated Chromophore Potentials. *Phys. Chem. Chem. Phys.* **2018**, *20*, 3310−3319.
(35) Matthews, B. W.; Fenna, R. E.; Bolognesi, M. C.; Schmid, M. F.; Olson, J. M. Structure of a Bacteriochlorophyll *a*-Protein from the Green Photosynthetic Bacterium *Prosthecochloris Aestuarii*. *J. Mol. Biol.* **1979**, *131*, 259−285.
(36) Kihara, S.; Hartzler, D.; Orf, G. S.; Blankenship, R. E.; Savikhin, S. The Fate of the Triplet Excitations in the Fenna-Matthews-Olson Complex and Stability of the Complex. *Biophys. J.* **2014**, *106*, 182a.
(37) Saito, S.; Higashi, M.; Fleming, G. R. Site-Dependent Fluctuations Optimize Electronic Energy Transfer in the Fenna−Matthews−Olson Protein. *J. Phys. Chem. B* **2019**, *123*, 9762.
(38) Khmelnitskiy, A.; Reinot, T.; Jankowiak, R. Impact of Single-Point Mutations on the Excitonic Structure and Dynamics in a Fenna−Matthews−Olson Complex. *J. Phys. Chem. Lett.* **2018**, *9*, 3378−3386.
(39) Fransted, K. A.; Caram, J. R.; Hayes, D.; Engel, G. S. Two-Dimensional Electronic Spectroscopy of Bacteriochlorophyll *a* in Solution: Elucidating the Coherence Dynamics of the Fenna-Matthews-Olson Complex Using Its Chromophore as a Control. *J. Chem. Phys.* **2012**, *137*, 125101.
(40) Blankenship, R. E.; Olson, J. M.; Miller, M. Antenna Complexes from Green Photosynthetic Bacteria. In *Anoxygenic Photosynthetic Bacteria*; Blankenship, R. E., Madigan, M. T., Bauer, C. E., Eds.; Springer Netherlands: Dordrecht, The Netherlands, 1995; pp 399−435.

https://doi.org/10.1021/acs.jpclett.3c01461
J. Phys. Chem. Lett. 2023, 14, 7038−7044

(41) Orf, G. S.; Blankenship, R. E. Chlorosome Antenna Complexes from Green Photosynthetic Bacteria. *Photosynth. Res.* **2013**, *116*, 315−331.
(42) Higgins, J. S.; et al. Photosynthesis Tunes Quantum-Mechanical Mixing of Electronic and Vibrational States to Steer Exciton Energy Transfer. *Proc. Natl. Acad. Sci. U. S. A.* **2021**, *118*, No. e2018240118.
(43) Khmelnitskiy, A.; Saer, R. G.; Blankenship, R. E.; Jankowiak, R. Excitonic Energy Landscape of the Y16F Mutant of the Chlorobium Tepidum Fenna−Matthews−Olson (FMO) Complex: High Resolution Spectroscopic and Modeling Studies. *J. Phys. Chem. B* **2018**, *122*, 3734−3743.
(44) Khmelnitskiy, A.; Kell, A.; Reinot, T.; Saer, R. G.; Blankenship, R. E.; Jankowiak, R. Energy Landscape of the Intact and Destabilized FMO Antennas from C. Tepidum and the L122Q Mutant: Low Temperature Spectroscopy and Modeling Study. *Biochim. Biophys. Acta - Bioenerg.* **2018**, *1859*, 165−173.
(45) Saer, R.; Orf, G. S.; Lu, X.; Zhang, H.; Cuneo, M. J.; Myles, D. A. A.; Blankenship, R. E. Perturbation of Bacteriochlorophyll Molecules in Fenna−Matthews−Olson Protein Complexes through Mutagenesis of Cysteine Residues. *Biochim. Biophys. Acta - Bioenerg.* **2016**, *1857*, 1455−1463.
(46) Maiuri, M.; Ostroumov, E. E.; Saer, R. G.; Blankenship, R. E.; Scholes, G. D. Coherent Wavepackets in the Fenna−Matthews−Olson Complex Are Robust to Excitonic-Structure Perturbations Caused by Mutagenesis. *Nat. Chem.* **2018**, *10*, 177−183.
(47) Magdaong, N. C. M.; Saer, R. G.; Niedzwiedzki, D. M.; Blankenship, R. E. Ultrafast Spectroscopic Investigation of Energy Transfer in Site-Directed Mutants of the Fenna−Matthews−Olson (FMO) Antenna Complex from Chlorobaculum Tepidum. *J. Phys. Chem. B* **2017**, *121*, 4700−4712.
(48) Saer, R. G.; Schultz, R. L.; Blankenship, R. E. The Influence of Quaternary Structure on the Stability of Fenna−Matthews−Olson (FMO) Antenna Complexes. *Photosynth. Res.* **2019**, *140*, 39−49.
(49) Gordon, M. S.; Slipchenko, L. V.; Li, H.; Jensen, J. H. The Effective Fragment Potential: A General Method for Predicting Intermolecular Forces. *Annu. Rep. Comput. Chem.* **2007**, *3*, 177−193.
(50) Slipchenko, L. V. Solvation of the Excited States of Chromophores in Polarizable Environment: Orbital Relaxation Versus Polarization. *J. Phys. Chem. A* **2010**, *114*, 8824−8830.
(51) Slipchenko, L. V. Effective Fragment Potential Method. In *Many-Body Effects and Electrostatics in Biomolecules*; Cui, Q., Meuwly, M., Ren, P., Eds.; CRC Press: Boca Raton, FL, 2016; pp 147−190.
(52) Slipchenko, L. V.; Gurunathan, P. K. Effective Fragment Potential Method: Past, Present, and Future. In *Fragmentation: Toward Accurate Calculations on Complex Molecular Systems*; Gordon, M. S., Ed.; Wiley, 2017; pp 183−208.
(53) DeFusco, A.; Minezawa, N.; Slipchenko, L. V.; Zahariev, F.; Gordon, M. S. Modeling Solvent Effects on Electronic Excited States. *J. Phys. Chem. Lett.* **2011**, *2*, 2184−2192.
(54) Gordon, M. S.; Smith, Q. A.; Xu, P.; Slipchenko, L. V. Accurate First Principles Model Potentials for Intermolecular Interactions. *Annu. Rev. Phys. Chem.* **2013**, *64*, 553−578.
(55) Gurunathan, P. K.; Acharya, A.; Ghosh, D.; Kosenkov, D.; Kaliman, I.; Shao, Y.; Krylov, A. I.; Slipchenko, L. V. Extension of the Effective Fragment Potential Method to Macromolecules. *J. Phys. Chem. B* **2016**, *120*, 6562−6574.
(56) Kim, Y.; Bui, Y.; Tazhigulov, R. N.; Bravaya, K. B.; Slipchenko, L. V. Effective Fragment Potentials for Flexible Molecules: Transferability of Parameters and Amino Acid Database. *J. Chem. Theory Comput.* **2020**, *16*, 7735−7747.
(57) Anda, A.; Hansen, T.; De Vico, L. Q_y and Q_x Absorption Bands for Bacteriochlorophyll *a* Molecules from LH2 and LH3. *J. Phys. Chem. A* **2019**, *123*, 5283−5292.

https://doi.org/10.1021/acs.jpclett.3c01461
J. Phys. Chem. Lett. 2023, 14, 7038−7044